Silicon Nanowire Solar Cells with µc-Si:H Absorbers for Radial Junction Devices

Letian Dai,* Martin Foldyna, Alvarez José, Isabelle Maurin, Jean-Paul Kleider, Thierry Gacoin, and Pere Roca i Cabarrocas

Silicon nanowire (SiNW) radial junction (RJ) solar cells using hydrogenated microcrystalline silicon (µc-Si:H) as absorber material have been studied. Since 2013, the performance of such RJ devices has been limited by the low fill factor (FF) and open-circuit voltage (V_{OC}). Thanks to the use of n-type hydrogenated microcrystalline silicon oxide (µc-SiO$_x$:H) as a bottom doped layer, the authors developed µc-Si:H RJ solar cells with a FF of 69.7% and a V_{OC} of 0.41 V yielding a power conversion efficiency of 4.1%, which is more than 40% higher than the previously published efficiency record of 2.9%. Herein, the role of n-type µc-SiO$_x$:H in the improvement of FF is highlighted.

1. Introduction

The use of hydrogenated microcrystalline silicon (µc-Si:H) as absorber material for photovoltaic (PV) applications has a long history and has led to a multitude of innovative results.[1–5] Its incorporation in core–shell silicon nanowires (NWs) was successfully realized in 2012 by Adachi.[6] These radial junction (RJ) devices demonstrated a better light-trapping with in particular a higher short-circuit current than thicker µc-Si:H planar devices. A drastic decrease in the reflectance, characterized by in situ spectroscopy ellipsometry, during the growth of SiNWs was observed.[7,8] However, the fill factor (FF) and the open-circuit voltage (V_{OC}) of RJ devices were slightly smaller than these measured on the planar reference device,[9] leading to an efficiency of 2.9% for these µc-Si:H RJs.

In spite of these low efficiency values, it must be kept in mind that the efficiency records of µc-Si:H planar solar cells are in the range of 8.6–11.9%.[10,11] Thus there is a strong potential for efficiency increase in µc-Si:H RJ solar cells, especially if we refer to other absorber thin-film technologies such as hydrogenated amorphous silicon (a-Si:H), which combined with RJs has demonstrated an efficiency of 9.2%[12] that is very close to the planar solar cell record of 10.3%.[13]

Our approach for optimizing the µc-Si:H p-i-n RJ is to replace p-type and n-type doped µc-Si:H layers by hydrogenated microcrystalline silicon oxide (µc-SiO$_x$:H). Indeed, as a doped layer commonly used in silicon thin-film solar cells, µc-SiO$_x$:H offers great interest: wider bandgap (1.9–2.9 eV),[14] low refractive index ($\approx$2)[15] and reasonably high conductivity (>1 S cm^{-1}).[16] Many studies in the past have used µc-SiO$_x$:H layers to improve the performance in thin films solar cells. Despeisse et al.[17] used a n-type doped µc-SiO$_x$:H as bottom doped layer in the n-i-p structure silicon solar cells and succeeded to increase the FF by 7.5%. A same finding for Kim et al.[18] that improved FF and V_{OC} by 4.7% and 3%, respectively, using n-type doped µc-SiO$_x$:H. In 2015, Misra et al.[12] used µc-SiO$_x$:H as a window layer in a-Si:H RJ solar cells, improving the short-circuit current density by 6.6%.

In this article, we have developed µc-Si:H RJs solar cells by implementing µc-SiO$_x$:H as doped layers. For this purpose, the structural, optical, and electrical properties of these layers were first studied in a planar configuration and then implemented on RJs SiNWs.

Dr. L. Dai, Dr. A. José, Prof. J.-P. Kleider
Laboratoire de Génie Electrique et Electronique de Paris
CentraleSupélec
CNRS
Université Paris-Saclay
Gif-sur-Yvette 91192, France
E-mail: letian.dai@geeps.centralesupelec.fr, letian.dai@outlook.com

Dr. L. Dai, Prof. J.-P. Kleider
Laboratoire de Génie Electrique et Electronique de Paris
CNRS
Sorbonne Université
Paris 75252, France

Dr. L. Dai, Dr. M. Foldyna, Prof. P. Roca i Cabarrocas
LPICM
CNRS
Ecole Polytechnique
Institut Polytechnique de Paris
Palaiseau 91128, France

Dr. L. Dai, Dr. A. José, Dr. I. Maurin, Prof. T. Gacoin
Physique de la Matière Condensée
CNRS
Ecole Polytechnique
Institut Polytechnique de Paris
Palaiseau 91128, France

The ORCID identification number(s) for the author(s) of this article can be found under https://doi.org/10.1002/pssa.202100231.

DOI: 10.1002/pssa.202100231

2. Experimental Section

Sample preparation started with 1 × 1 in.^{2} Corning glass (Cg) substrates (type 1737). The back contact structure was either Cg/ZnO:Al or Cg/Ag/ZnO:Al where ZnO:Al refers to aluminum-doped zinc oxide (ZnO) with a thickness of 120 nm and Ag refers to silver as a back reflector with a thickness of

160 nm. The layers of Ag and ZnO:Al were deposited via magnetron sputtering. Based on previous research experiences,[12,19,20] a very thin layer of Sn with a nominal thickness of ≈ 1 nm was deposited on the surface of ZnO:Al via vacuum evaporation ($<10^{-6}$ mbar). The metal Sn was used as the catalyst to grow SiNWs. After that, the samples were transferred into a plasma-enhanced chemical vapor deposition (PECVD) reactor dedicated to the growth of doped SiNWs. N-type doped SiNWs were fabricated at $\approx 410\,°C$ in the PECVD reactor with a capacitively coupled radio frequency (RF) discharge at 13.56 MHz, the gas sources of silane (SiH_4), hydrogen (H_2), and phosphine (PH_3) under a pressure of 2.15 mbar and a power density of 20 mW cm^{-2}. The gas flow rates of H_2, SiH_4, and PH_3 were 200, 5, and 0.4 sccm, respectively. As shown in S1—Figure S1, Supporting Information, the lengths of SiNWs were calibrated with the duration of growth.

After the growth of n-type SiNWs, the samples were transferred to another PECVD reactor[21] optimized for the deposition of thin-film layers with the objective of developing a n-i-p structure. A sequence of layers, namely n-type doped μc-SiO$_x$:H (≈ 20 nm) or n-type doped μc-Si:H (≈ 20 nm), intrinsic layer of μc-Si:H (≈ 375 nm), p-type doped μc-SiO$_x$:H (≈ 10 nm), and p-type doped μc-Si:H (≈ 10 nm) were deposited on SiNWs at the temperature of 150 °C. P-type and n-type films were, respectively, obtained by adding trimethylborane (TMB, 1% diluted in H_2) or phosphine (PH_3, 0.1% diluted in H_2). The oxide layers of n-type (or p-type) μc-SiO$_x$:H were made by adding CO_2 as the O source into the mixture gas of SiH_4, H_2 and PH_3 (or TMB) during the PECVD process. All these effective thicknesses were estimated through a previous study that aimed to calibrate the thickness of the thin-film shell layer on SiNW core. This calibration process has been carried out with respect to reference planar layers deposited on Cg glass substrates (see S2—Figure S2, Supporting Information).

The top layer of the RJ solar cells was made of indium tin oxide (ITO) used as a front transparent electrode with a thickness of ≈ 160 nm. This layer was deposited using magnetron sputtering at the pressure of 6.3×10^{-3} mbar with a RF power of 200 W for 7 min at room temperature under a shadow mask. The contact area of ITO was circular with a diameter of 4 mm.

For this study, we have prepared four samples (n_1, n_2, n_3, and n_4), the structure of which from bottom to top is shown in **Table 1**. The difference between samples n_1 and n_2 was that n_1 used n-type doped μc-Si:H, whereas n_2 used n-type doped μc-SiO$_x$:H. For sample n_3, we added a silver (Ag) back reflector

between Cg and ZnO:Al, and for sample n_4, we decreased the length of SiNWs from ≈ 800 to ≈ 500 nm.

Before current density–voltage (J–V) and external quantum efficiency (EQE) characterizations, the RJ solar cells were annealed at 200 °C for 15 min. The J–V characterizations were done under the global AM 1.5 sunlight illumination (100 mW cm^{-2}). The EQE characterizations were done using a Fourier transform photocurrent spectroscopy (FTPS) set-up[22] adapted from a FTIR spectrometer (Thermo Scientific, Nicolet iS50 FTIR Spectrometer).

A substantial part of this study was initially conducted on planar layer samples deposited on Cg as references. In this way, we have characterized several groups of planar layers, namely n-type doped μc-SiO$_x$:H, intrinsic μc-Si:H, p-type doped μc-SiO$_x$:H, and p-type doped μc-Si:H. The preparation conditions of these materials are shown in Supporting Information (S3). The crystalline fraction and electrical properties were characterized using Raman spectroscopy (HORIBA, LabRAM HR Evolution), and four-probe measurements. The illustrations of these characterizations are shown in the Supporting Information (S4—Figure S3 and Figure S4).

The morphologies of SiNWs and RJs were characterized by scanning electron microscopy (SEM, Hitachi S4800 FEG-SEM, acceleration voltage: 10 kV). The density of SiNWs was analyzed by applying ImageJ software[23] to the SEM images.

3. Results and Discussion

3.1. Electrical and Optical Properties of Reference Planar Layers on Cg

To estimate the electrical and optical properties of the thin-film layers sequentially deposited on SiNWs, we characterized them in the planar configuration, as previously explained. In S4—Figure S3, Supporting Information, from the Raman characterization results, the crystalline fraction of intrinsic and p-type doped μc-Si:H, n-type doped, and p-type doped μc-SiO$_x$:H were calculated at about 68%, 54%, 45%, and 18%, respectively. The conductivity of these layers versus the temperature is shown in S4—Figure S4, Supporting Information. The Arrhenius plots highlight an activation energy of 621 ± 30 meV for the intrinsic μc-Si:H, which is close to half the bandgap of this material. The activation energies of the p-type μc-Si:H, n-type and p-type μc-SiO$_x$:H layers reveal low activation energies of 19.2 ± 0.5, 79.2 ± 0.9, and 94.1 ± 2.2 meV, respectively.

3.2. Morphology Characterization of SiNWs and RJ Structure

The evolution of the morphology of the devices, from bare NWs to the finalized RJ structure, was analyzed by SEM. SEM images of n-type SiNWs with a density of $\approx 6 \times 10^8$ cm^{-2}, a diameter of ≈ 40 nm and a length of ≈ 500 nm are shown in **Figure 1**a. After the deposition of n–i–p and ITO layers, SEM images of RJs with a diameter of ≈ 820 nm and a density of $\approx 0.7 \times 10^8$ cm^{-2} are shown in Figure 1b. Regarding the final density, it has been reduced by almost one order of magnitude pointing out NW coalescence taking place during the RJ fabrication.[24]

Table 1. Structure details for samples n_1–n_4 from bottom to top.

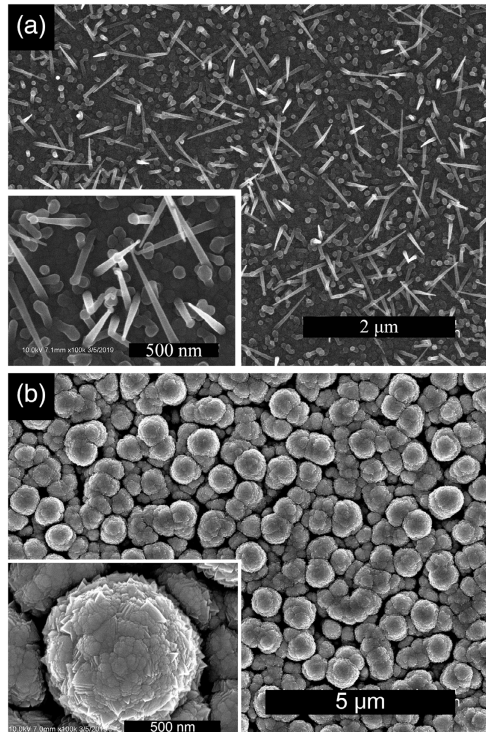| Samples	bottom	→		top
n1	Cg/ ZnO:Al	SiNWs (n) ~800 nm	μc-Si:H(n)	μc-Si:H(i)/
n2			μc-SiO$_x$:H(n)	μc-SiO$_x$:H(p)/
n3	Cg/ Ag/ZnO:Al			μc-Si:H(p+)/
n4		SiNWs (n) ~500 nm		ITO

Figure 1. a) SEM image of SiNWs grown on ZnO:Al surface, the inset shows a high magnification image of SiNWs. The scale bars correspond to 2 μm and 500 nm, respectively. b) SEM image of complete μc-Si:H RJ with ITO coating, the inset shows a high magnification image of the RJs. The scale bars correspond to 5 μm and 500 nm, respectively.

3.3. FF improvement

Figure 2 shows the J–V curve and EQE spectra of the RJ solar cell samples (n_1–n_4). Note that the device surface area is 12.6 mm^2. The detailed performances of samples n_1–n_4 are shown in **Table 2**. Fitted series resistance R_s and shunt resistance R_{sh} were determined from the slopes of the J–V curves at $V = 0$ and $V = V_{OC}$ under illumination in Figure 2a using "Slope method."[25]

As shown in Table 1, sample n_1 differs from the others in that the n-doped layer is μc-Si:H instead of μc-SiO$_x$:H, and leads to a device with the poorest performances (Table 2).

The low FF value evidenced for n_1 seems to be mostly associated with a low shunt resistance value (see Table 2). Replacing the n-type doped μc-Si:H by a wider bandgap material, i.e., n-type doped μc-SiO$_x$:H, greatly improves the FF, in particular by increasing the shunt resistance from 9 to 277 Ω cm^2.

When comparing samples n_2, n_3, and n_4, all three of which include n-type and p-type μc:SiO$_x$:H layers, a large J_{SC} difference can be seen between the n_2 sample and the others. Indeed, sample n_2 is the only one in this series that does not have an Ag back reflector, highlighting its importance even in the context of NW structures that efficiently trap light.

Samples n_3 and n_4 are the RJ devices displaying the best performances. A higher J_{SC} was obtained for n_3 due to the fact that
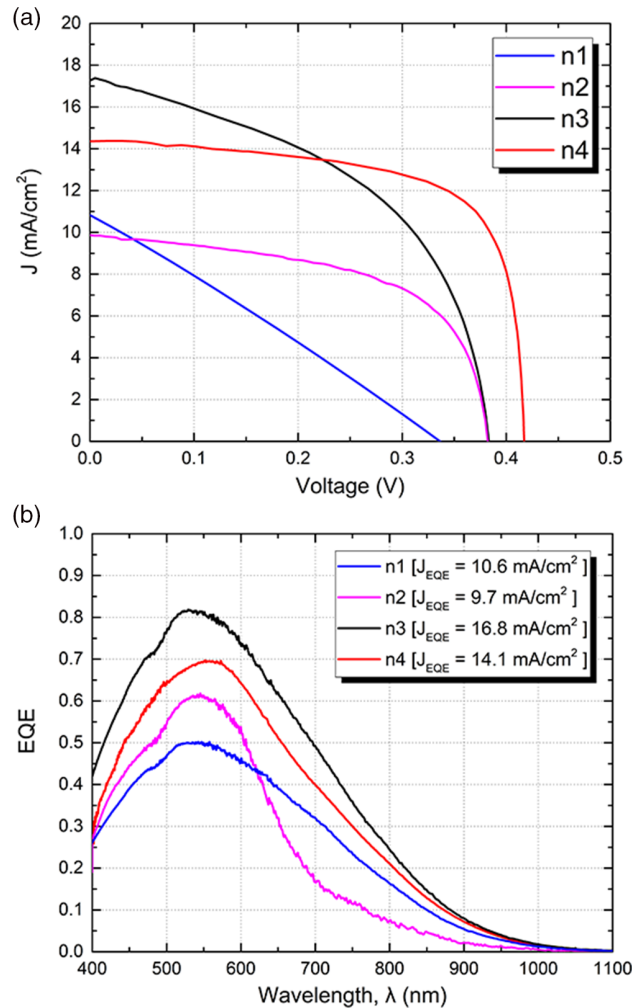

Figure 2. Performance of samples n_1–n_4 RJ solar cells. a) J–V characteristics under AM 1.5 global illumination (100 mW/cm^2). b) EQE spectra of samples n_1–n_4 RJ.

Table 2. Solar cell parameters of samples n_1–n_4.

Sample	V_{OC} [V]	J_{SC} [mA cm^{-2}]	FF [%]	R_s [Ω cm^{-2}]	R_{sh} [Ω cm^{-2}]	η [%]
n_1	0.34	10.9	26.6	27.6	9	0.99
n_2	0.39	9.8	57.8	2.3	277	2.21
n_3	0.38	17.3	49.3	2.3	78.3	3.24
n_4	0.41	14.4	69.7	0.7	781	4.13

the SiNWs were longer (800 nm compared with 500 nm). However, V_{OC} and FF reveal the best improvements when reducing the length to 500 nm (case of sample n_4). This suggests issues of nonconformal coverage for longer NWs, already observed by other studies,[26–28] due to coalescence of NWs and shadowing effects.

The sample n_4 with NWs length of 500 nm shows the highest power conversion efficiency reported so far, with the following solar cell parameters: $J_{SC} = 14.4$ mA cm^{-2}, FF = 69.7%,

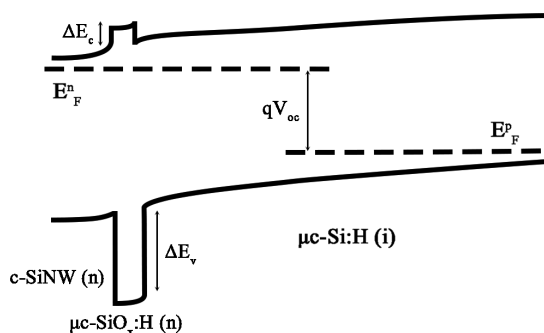**Figure 3.** Schematic drawing of band diagram of the n–i (from n-type to intrinsic) junction with the n-type μc-SiO$_x$:H as the bottom doped layer under the illumination.

$V_{OC} = 0.41$ V, and $\eta = 4.1\%$. As illustrated in S4—Figure S5, Supporting Information, the devices studied in sample n_4 show a homogeneous V_{OC} around 0.41–0.42 V, whereas J_{SC} and FF show a variation of less than 10%.

The EQE spectra of samples n_1–n_4 are shown in Figure 2b and match well the expected absorption range of μc-Si:H solar cells.[10,11] The extracted short-circuit current density, named J_{EQE} is the integrated current density of the EQE spectra in Figure 2b, which agrees to the J_{SC} obtained from J–V measurements with less than 3% difference.

Compared with the results of Adachi et al.,[9] the most significant improvement of our RJ devices concerns the FF, which is almost 40% higher thanks to the use of μc-SiO$_x$:H doped layers instead of μc-Si:H ones. Note that the distribution and the orientation of SiNWs are random, as shown in Figure 1a, implying that electrical interconnections may form during the fabrication of the RJ[12,19,20,27] and results in the degradation of the shunt resistance. The use of μc-SiO$_x$:H seems more favorable to minimize the effects of interconnection, and has in particular improved the V_{OC}. The latter point has also been studied and reported for other types of thin-film solar cells.[16,17,29] To understand the higher V_{OC} and shunt resistance of the cells incorporating a n-type μc-SiO$_x$:H layer, let us consider the energy bandgap diagram of the n–i–p junction, as schematically shown in **Figure 3**. The introduction of the μc-SiO$_x$:H layer leads to the presence of a significant valence band offset barrier that repels the holes generated in the intrinsic μc-Si:H layer reducing the recombination at the interface with the c–SiNW (n) core, therefore improving both FF and V_{OC}.

4. Conclusions

In this study, we have fabricated SiNW RJ solar cells with μc-Si:H as absorber material. We have developed and implemented μc-SiO$_x$:H doped layers to replace standard μc-Si:H. This approach has been particularly efficient to increase the shunt resistance and the V_{OC}. Ag back reflector has demonstrated to be necessary to strongly increase J_{SC} values. Finally, reducing the length of the NWs resulted in a solar cell efficiency of 4.1%, which is the best efficiency reported so far for the μc-Si:H RJ technology. These results show that there is a strong potential for improvement,

in particular by focusing on adjusting density and length of SiNWs for an optimized conformal coverage.

[1] S. Usui, M. Kikuchi, *J. Non-Cryst. Solids* **1979**, *34*, 1.
[2] J. Meier, R. Flückiger, H. Keppner, A. Shah, *Appl. Phys. Lett.* **1994**, *65*, 860.
[3] A. Matsuda, in *Journal of Non-Crystalline Solids*, Elsevier, North-Holland **2004**, pp. 1–12.
[4] P. Roca i Cabarrocas, A. Fontcuberta i Morral, B. Kalache, S. Kasouit, in *Solid State Phenomena*, Trans Tech Publications Ltd, Uetikon **2003**, pp. 257–268.
[5] B. Rech, T. Repmann, M. N. van den Donker, M. Berginski, T. Kilper, J. Hüpkes, S. Calnan, H. Stiebig, S. Wieder, *Thin Solid Films* **2006**, *511–512*, 548.
[6] M. M. Adachi, *Development and Characterization of PECVD Grown Silicon Nanowires for Thin Film Photovoltaics*, UWSpace **2012**, http://hdl.handle.net/10012/6873.
[7] L. Yu, B. O'Donnell, P. J. Alet, P. Roca i Cabarrocas, *Sol. Energy Mater. Sol. Cells* **2010**, *94*, 1855.
[8] Z. Mrazkova, M. Foldyna, S. Misra, M. Al-Ghzaiwat, K. Postava, J. Pištora, P. Roca i Cabarrocas, *Appl. Surf. Sci.* **2017**, *421*, 667.
[9] M. M. Adachi, M. P. Anantram, K. S. Karim, *Sci. Rep.* **2013**, *3*, 1.
[10] K. Ishizaki, M. De Zoysa, Y. Tanaka, T. Umeda, Y. Kawamoto, S. Noda, *Opt. Express* **2015**, *23*, A1040.
[11] H. Sai, T. Matsui, K. Kumagai, K. Matsubara, *Appl. Phys. Express* **2018**, *11*, 022301.
[12] S. Misra, L. Yu, M. Foldyna, P. Roca i Cabarrocas, *IEEE J. Photovoltaics* **2015**, *5*, 40.

[13] A. Lambertz, F. Finger, R. E. I. Schropp, U. Rau, V. Smirnov, *Prog. Photovoltaics Res. Appl.* **2015**, *23*, 939.

[14] V. Smirnov, A. Lambertz, S. Tillmanns, F. Finger, *Can. J. Phys.* **2014**, *92*, 932.

[15] S. J. Jung, B. J. Kim, M. Shin, *Sol. Energy Mater. Sol. Cells* **2014**, *121*, 1.

[16] A. Lambertz, F. Finger, B. Holländer, J. K. Rath, R. E. I. Schropp, in *Journal of Non-Crystalline Solids*, Elsevier, North-Holland **2012**, pp. 1962–1965.

[17] M. Despeisse, G. Bugnon, A. Feltrin, M. Stueckelberger, P. Cuony, F. Meillaud, A. Billet, C. Ballif, *Appl. Phys. Lett.* **2010**, *96*, 073507.

[18] S. Kim, H. Lee, J. W. Chung, S. W. Ahn, H. M. Lee, *Curr. Appl. Phys.* **2013**, *13*, 743.

[19] L. Yu, P.-J. Alet, G. Picardi, I. Maurin, P. Roca i Cabarrocas, *Nanotechnology* **2008**, *19*, 485605.

[20] S. Misra, L. Yu, M. Foldyna, P. Roca i Cabarrocas, *Sol. Energy Mater. Sol. Cells* **2013**, *118*, 90.

[21] P. Roca i Cabarrocas, J. B. Chévrier, J. Huc, A. Lloret, J. Y. Parey, J. P. M. Schmitt, *J. Vac. Sci. Technol. A Vacuum, Surfaces, Film.* **1991**, *9*, 2331.

[22] N. Puspitosari, C. Longeaud, R. Lachaume, L. Zeyu, R. Rusli, P. Roca i Cabarrocas, in *Physica Status Solidi. C, Current Topics in Solid State Physics*, Wiley-VCH Verlag, Weinheim **2017**, p. 1700165.

[23] W. S. Rasband, http://imagej.nih.gov/ij/ (accessed: June 2021), **2011**.

[24] J. Tang, J.-L. Maurice, W. Chen, S. Misra, M. Foldyna, E. V. Johnson, P. Roca i Cabarrocas, *Nanoscale Res. Lett.* **2016**, *11*, 455.

[25] C. Chibbaro, M. Zimbone, G. Litrico, P. Baeri, M. L. Lo Trovato, F. Aleo, *J. Appl. Phys.* **2011**, *110*, 044505.

[26] L. Yu, B. O'Donnell, M. Foldyna, P. Roca i Cabarrocas, *Nanotechnology* **2012**, *23*, 194011.

[27] M. Müller, M. Ledinský, J. Kočka, A. Fejfar, J. Červenka, *J. Vac. Sci. Technol. B, Nanotechnol. Microelectron. Mater. Process. Meas. Phenom.* **2018**, *36*, 011401.

[28] M. Macias-Montero, A. N. Filippin, Z. Saghi, F. J. Aparicio, A. Barranco, J. P. Espinos, F. Frutos, A. R. Gonzalez-Elipe, A. Borras, *Adv. Funct. Mater.* **2013**, *23*, 5981.

[29] M. Python, E. Vallat-Sauvain, J. Bailat, D. Dominé, L. Fesquet, A. Shah, C. Ballif, *J. Non-Cryst. Solids* **2008**, *354*, 2258.

2100231 (5 of 5)